Nuclear Instruments and Methods in Physics Research A 763 (2014) 314–319

Contents lists available at ScienceDirect

Nuclear Instruments and Methods in Physics Research A

journal homepage: www.elsevier.com/locate/nima

A broad angular-range measurement of elastic and inelastic scatterings in the ^{16}O on ^{27}Al reaction at 17.5 MeV/u

F. Cappuzzello [a,b,*], C. Agodi [a], M. Bondì [a,b], D. Carbone [a,b], M. Cavallaro [a], A. Cunsolo [a,b], M. De Napoli [c], A. Foti [b,c], D. Nicolosi [a,b], S. Tropea [a,b], P.N. de Faria [d], R. Linares [e], J.R.B. Oliveira [d], M.R.D. Rodrigues [d]

[a] INFN - Laboratori Nazionali del Sud, Via S. Sofia 62, I-95125 Catania, Italy
[b] Dipartimento di Fisica e Astronomia, Università di Catania, Via S. Sofia 64, I-95125 Catania, Italy
[c] INFN - Sezione di Catania, Via S. Sofia 64, I-95125 Catania, Italy
[d] Universidade de São Paulo, Departamento de Física Nuclear, Instituto de Física da Universidade de São Paulo, Caixa Postal 66318, 05315-970 São Paulo, SP, Brazil
[e] Instituto de Física, Universidade Federal Fluminense, Litoranea s/n, Gragoatá, Niterói, Rio de Janeiro 24210-340, Brazil

ARTICLE INFO

Article history:
Received 10 March 2014
Received in revised form
16 June 2014
Accepted 18 June 2014
Available online 27 June 2014

Keywords:
Elastic scattering
Magnetic spectrometers
Superconducting cyclotrons
Trajectory reconstruction

ABSTRACT

The elastic and inelastic scattering of ^{16}O ions on ^{27}Al target nuclei were measured in a broad angular range ($5^\circ < \theta_{lab} < 40^\circ$) at 280 MeV incident energy. The beam was accelerated by the K800 Superconducting Cyclotron at the INFN-LNS laboratory. The ejectiles were detected by the MAGNEX large acceptance magnetic spectrometer. The matching of the beam properties with the optical characteristics of the spectrometer allowed to separate the elastic from the inelastic channels in the energy spectra and measure accurate cross-section distributed over more than eight orders of magnitude down to a few tens of nb/sr.

1. Introduction

Recently a renewed interest in studies of heavy-ion elastic and inelastic scattering above the Coulomb barrier has been driven by the predictions of new phenomena, as result of state of the art reaction calculations based on the coupled channel theory [1]. In particular the appearance of a new kind of rainbow pattern in the cross-section angular distributions, connected to the sizeable coupling of the elastic and inelastic channels, was predicted for many colliding nuclei. First evidences were found in recent experiments at 100 MeV beam energy [2,3]. According to the calculations this phenomenon should be more evident with the increase of the incident energy [4]. However such experiments require very stringent conditions on mass, energy and angular resolution, and accuracy for an unambiguous selection of the elastic scattering events. In particular the requirement of high energy resolution, necessary to separate elastic from inelastic channels, is one of the hardest to be fulfilled when the incident energy is increased.

The use of electrostatic accelerators such as a Tandem Van der Graaff, appropriate for high resolution experiments, is not an option for heavy ions at energies of ~15 MeV/u or higher, where the nuclear rainbow is predicted to be more pronounced. On the other hand, Cyclotrons or LINAC accelerators for heavy ions are typically not designed for high energy resolution experiments. A possibility could be offered by spectrometers based on the dispersion matching with the beam line [5,6], which do guarantee an excellent compensation of the beam energy spread, also at high bombarding energies. However these devices have small solid angle and require wide area targets. This is inconvenient when the cross-sections are very low and thin targets are needed to preserve the energy resolution, as it happens in heavy-ion collision experiments. Nowadays finding a solution to these problems represents the major technical challenge for the research on nuclear rainbow scattering with heavy ions or for high resolution multi-nucleon transfer reactions [7].

In this paper we describe the experimental technique and the data analysis methods used to successfully face the above challenges. In particular, the application to the $^{16}O+^{27}Al$ elastic and inelastic scattering at 280 MeV will be presented and discussed. The basic feature is the use of the K800 Superconducting Cyclotron (SC) [8] accelerator of the INFN-LNS laboratory in Catania and the

* Corresponding author at: INFN - Laboratori Nazionali del Sud, Via S. Sofia 62, I-95125 Catania, Italy. Tel.: +39 95 542384.
E-mail address: cappuzzello@lns.infn.it (F. Cappuzzello).

http://dx.doi.org/10.1016/j.nima.2014.06.058
0168-9002/

MAGNEX large acceptance magnetic spectrometer [9–11] for the detection of the ejectiles. A key aspect of the experiment is the matching of the beam characteristics with the spectrometer optics. This is made possible, for the first time with a CS heavy-ion beam, the application of the powerful technique of ray reconstruction, implemented in MAGNEX for the determination of the ejectiles motion [12]. It will be shown that energy spectra and angular distributions are extracted with adequate resolution and accuracy for frontier research activity on these topics.

2. The experiment

The $^{16}O^{3+}$ beam was accelerated by the INFN-LNS SC accelerator at 280 MeV total incident energy. A set of remotely controlled slits was mounted in the focal plane of a beam line bending magnet to perform a momentum selection, while checking the transmitted beam current. Two series of diaphragms, mounted 0.15 m and 2 m upstream the target, limited the beam spot on the target to 1.2 mm in horizontal (dispersive) and 2.3 mm in the vertical direction. The angular divergence at the target, defined by the same system, was $\Delta\theta_b \sim 0.05^\circ$ horizontally and $\Delta\varphi_b \sim 0.17^\circ$ vertically. A fine tuning of the accelerator allowed to extract a single turn beam of about 10 pnA. The beam current was monitored by a Faraday cup (4 cm deep) having a circular aperture (8 mm diameter) and an electron suppression ring, mounted downstream in the MAGNEX scattering chamber.

A ^{27}Al 109 ± 5 μg/cm^2 self-supporting target located in the scattering chamber was used. According to the kinematics the contribution of the beam divergence to the overall energy spreading for ^{16}O elastically scattered ions from the ^{27}Al target is less than 150 keV at the largest explored angles and smaller at the most forward angles. The collimation system was aligned to guarantee that the beam intercepted the target along the spectrometer optical axis, thus providing the best matching between the beam transport and the spectrometer optics. An accuracy of ± 0.1 mm in the definition of the spectrometer object point and $\pm 0.003^\circ$ in the beam direction were obtained, thanks to the use of a high precision bubble level and theodolite for the alignment of the upstream diaphragms and the target ladder. Under these conditions the effect of the misalignment of the beam as compared to the spectrometer object point on the momentum resolution is negligible [12].

The scattered ejectiles were momentum analyzed by the spectrometer and detected by the Focal Plane Detector (FPD) [13,14]. The magnetic field of the dipole magnet of the spectrometer was set in order that the trajectories of the elastically scattered $^{16}O^{8+}$ ions were transmitted with a magnetic rigidity 5% larger than the optical axis. For each angular setting the strength of the quadrupole magnet was adjusted in order to get a slight under-focusing condition for the trajectories corresponding to the elastic channel. This strategy prevented the point to parallel optical conditions in the vertical direction, thus preserving the best resolution in the reconstructed vertical angle. In the different experimental runs, the optical axis of the spectrometer was centered at the angles $\theta_{opt} = 10^\circ$, 13°, 18°, 26° and 34°. In all the runs the ejectile trajectories were accepted between -5.2° and $+6.3^\circ$ in the horizontal and $\pm 7.1^\circ$ in the vertical directions, with respect to the optical axis. An angular overlap of more than 6° between two contiguous sets of measurements was thus available. The beam intensity was about 10 pnA for the runs at the largest angles, being reduced down to 0.2 pnA at $\theta_{opt} = 10^\circ$ to avoid distortions in the FPD response due to the high rate concentrated in the region of the elastic trajectories. The FPD was filled with 99.95% pure isobutane at 15 mbar pressure. A voltage of -1200 V was applied to the cathode and $+760$ V to the multiplication wires. Under such working conditions the FPD allows the identification of the detected ions in atomic and mass number and electric charge. In particular the measurement of the horizontal position (X_{foc}) and angle (θ_{foc}), the energy loss corrected by the trajectory length inside the active volume (ΔE_{CP}^{corr}) and the residual energy (E_{resid}) are used to this purpose, according to the technique described in Ref. [15]. Fig. 1 shows an example of the clear separation achieved for the ^{16}O ions in this work.

The FPD also measures the horizontal and vertical impact position (X_{foc}, Y_{foc}) and direction (θ_{foc}, ϕ_{foc}) of the ion trajectories at the focal plane [13,16]. An example of the two-dimensional histogram of the measured θ_{foc} versus X_{foc} and Y_{foc} versus X_{foc} for the experimental setting at $\theta_{opt} = 18^\circ$ is shown in Fig. 2. The correlated loci in the plots indicate the population of the ground state at about $X_{foc} = 0.2$ m and of the excited states of ^{27}Al at smaller X_{foc}. The curvature of the loci is due to both the kinematic effect and the aberrations in the horizontal phase space. The loci with different curvatures represent the population of the states of ^{12}C and ^{16}O nuclei present as impurities of the target.

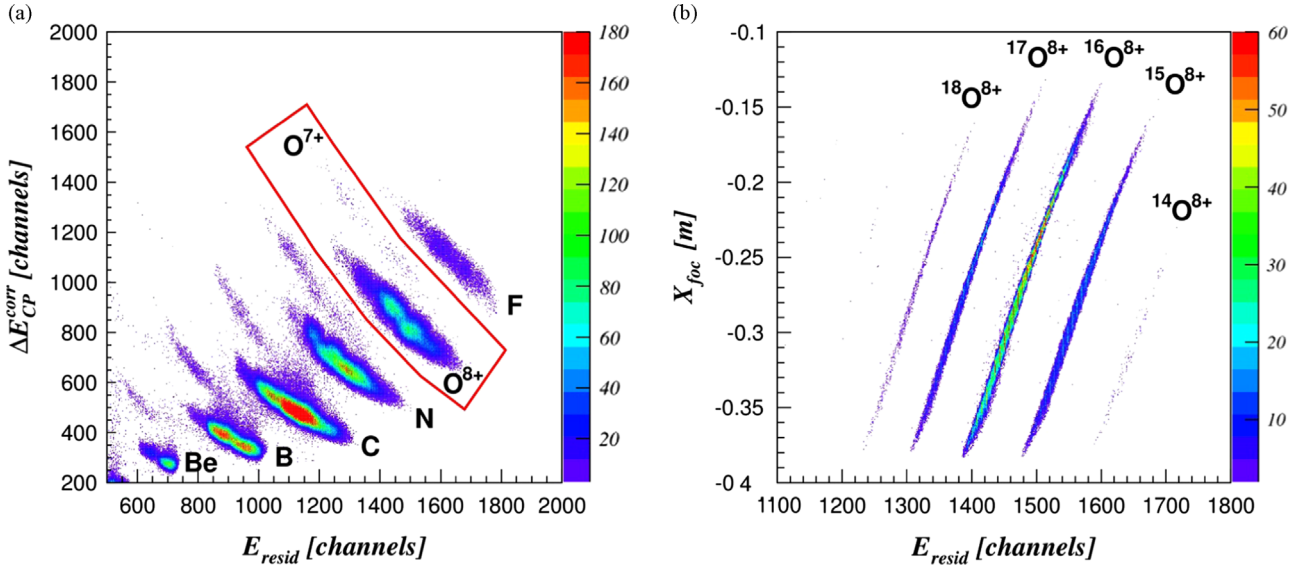

Fig. 1. Two-dimensional spectra measured in the $^{16}O + ^{27}Al$ reaction at 280 MeV and scattering angle $13^\circ < \theta_{lab} < 24^\circ$. (a): $\Delta E_{CP}^{corr} - E_{resid}$ plot. The group of the oxygen ions is encircled with a contour line. (b): $X_{foc} - E_{resid}$ plot for the selected oxygen isotopes.

The θ_{foc} values are distributed around 1.033 rad to account for the FPD inclination with respect to the plane perpendicular to the optical axis [13]. The lines of reduced efficiency in the left panel correspond to the lateral overlap region between two contiguous columns of the FPD silicon detectors. The horizontal lines of reduced efficiency in the right panel correspond to the shadow generated in the FPD by the 0.8 mm diameter supporting wires of the entrance detector window.

The measured ion positions and angles were used as input of the high order ray-reconstruction algorithms, according to the procedures described in Ref. [12,17]. This technique guarantees an effective compensation of the aberrations generated by the large aperture magnetic elements of the spectrometer [10,11]. As a result the phase space parameters are reconstructed back to the target point for the selected ^{16}O ejectiles. These are then transformed, by the application of relativistic two-body kinematics relations, in the scattering angle and kinetic energy of the detected ejectiles. In this procedure the masses of ^{27}Al residue and ^{16}O ejectile are assumed for all the events, with the consequence that the events relative to different processes generate loci with apparently unphysical behavior in this representation. Fig. 3 shows two examples of reconstructed parameters for the $^{16}O^{8+}$ reaction ejectiles. In particular the scattering angle θ_{lab} is shown versus the excitation energy E_x. The ^{27}Al ground and some of the low lying excited states are visible as vertical and straight loci, as expected since the excitation energy of the populated states does not depend on the scattering angle. The population of the four bound excited states of ^{16}O ejectiles at 6.05, 6.13, 6.92 and 7.12 MeV is also possible. However no clear evidence of such transitions is found in the data, likely due to the low polarizability of the doubly magic ^{16}O nucleus. The loci with a tilted trend in Fig. 3 represents the events relative to the scattering on ^{16}O and ^{12}C contaminants in the target. The distinct curvatures are due to the different kinematics of ^{16}O scattering on the ^{16}O and ^{12}C target nuclei.

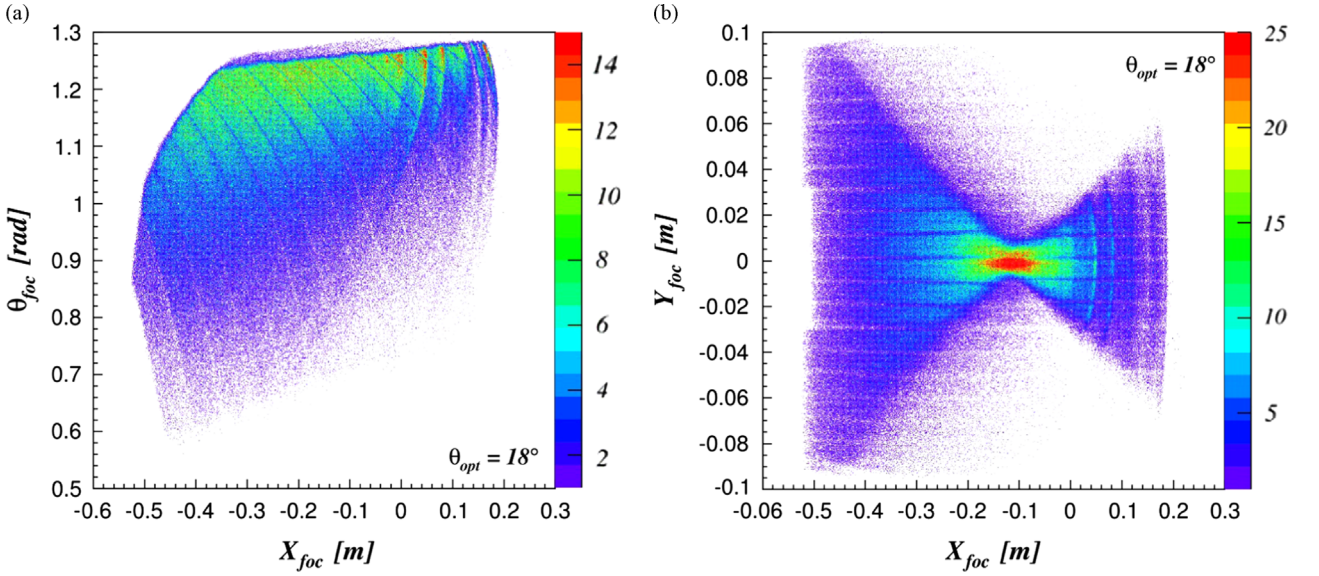

Fig. 2. Plot of the horizontal angle (panel a) and vertical position (panel b) against the horizontal position measured at the focal plane for the $^{16}O^{8+}$ ejectiles of the ^{27}Al(^{16}O, ^{16}O)^{27}Al scattering at 280 MeV and $13^\circ < \theta_{lab} < 24^\circ$. The coordinates of the optical axis are (X_{foc}=0; θ_{foc}=1.033) in the left panel and (X_{foc}=0; Y_{foc}=0) in the right panel.

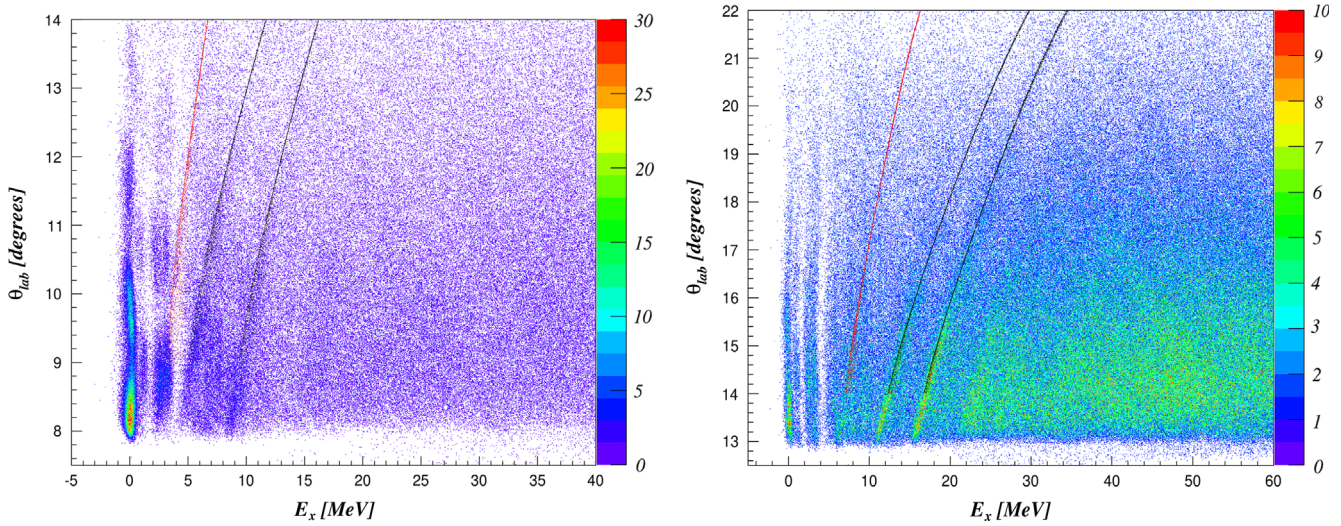

Fig. 3. Two-dimensional plot of the reconstructed θ_{lab} versus the ^{27}Al excitation energy E_x for the ^{27}Al(^{16}O, ^{16}O)^{27}Al reaction at 280 MeV and θ_{opt}=13° (left panel) and 18° (right panel). The red points represent the calculated kinematics for the population of the ^{16}O ground state. The black points represent the population of ^{12}C ground state and the excited state at 4.439 MeV.(For interpretation of the references to color in this figure legend, the reader is referred to the web version of this article.)

3. Energy resolution

The spread in the reconstructed excitation energy parameter is mainly generated by four independent sources: the momentum distribution of the beam, the kinematic broadening due to the finite angular resolution, the atomic multiple scattering of the beam ions and ejectiles in the target and the spectrometer finite momentum resolution. The multiple scattering effect in the target slowly decreases as a function of the beam energy whereas the other sources give approximately linearly increasing energy spread at increasing incident energy ($\Delta E \propto E$). A careful optimization of each contribution was thus needed in order to get the necessary resolution at least for the separation of the elastic scattering from the inelastic excitation of ^{27}Al at 844 keV.

Under the accelerator working conditions set for the experiment (45 kV accelerating voltage, $^{16}O^{3+}$ accelerated ions, second harmonic, six accelerating gaps) an energy difference of 0.25% (corresponding to ~700 keV) among two consecutive beam turns was estimated at the extraction of the accelerator. Under such conditions even two extracted orbits would have produced an intolerable experimental condition. However, thanks to the single orbit selection, the beam energy spread was limited to ~0.1%, corresponding to ~280 keV (Full Width at Half Maximum). This spread was mainly determined by the small ripple of the magnetic field strength and the stability of Radio Frequency (RF) inside the SC.

The kinematic energy broadening is critically connected to the achievable angular resolution and is particularly important at large scattering angles θ_{lab}. Considering the beam geometry described above ($\Delta\theta_b \sim 0.05^\circ$), the overall angular spread is mainly determined by the limited spectrometer angular resolution ($\Delta\theta_S \sim 0.2^\circ$). As an example, for the ^{27}Al(^{16}O, ^{16}O)^{27}Al reaction at 280 MeV incident energy, considering an angular spread of 0.2°, an energy broadening of ~100 and 600 keV is obtained at $\theta_{lab}=5^\circ$ and $\theta_{lab}=40^\circ$, respectively. Special care was therefore taken in the optimization of the angular resolution, especially at large θ_{lab}, where the polar angle is mainly determined by the horizontal Cartesian component. In particular the reduction of the voltage of the multiplication wires of the FPD to +740 V, in the runs at the largest angles, guaranteed a minimization of the inter-pad cross talk, which is known to have a relevant influence on the tracking accuracy for very inclined trajectories at the focal plane [16].

As stated in Ref. [18], the choice of the target thickness was the result of a careful compromise between the energy spread induced by the beam-target interaction and reaction yield constraints. For this purpose the target ladder was rotated 20° about the vertical axis in the same sense of the spectrometer angle. This minimized the spreading due to the different energy losses between the ^{16}O ejectiles scattered at different depths inside the target. An overall contribution ranging from 60 keV (at $\theta_{lab}=5^\circ$) to 120 keV ($\theta_{lab}=40^\circ$) was calculated by the SRIM code [19] under this condition. The spectrometer intrinsic energy resolution is known to be as high as 1/1000, corresponding to ~280 keV in ^{27}Al excitation energy [12].

According to the above discussion, the expected overall energy resolution is about 450 keV at forward angles. Fig. 4 shows that the measured full width at half maximum, extracted from a fit assuming a two-Gaussian model, is 460 ± 20 keV at $7^\circ < \theta_{lab} < 8^\circ$. This demonstrates that the single turn beam was actually selected and that the spectrometer response was as good as that known at lower energies. At the largest angles, due to the dominant effect of the kinematic broadening, the overall resolution is expected to be lower (~ 660 keV at 30° and ~740 keV at 40°). The fit in Fig.4 gives $\sim 650 \pm 200$ keV, thus confirming the expectations.

Despite the eight orders of magnitude difference (see next section) in the elastic cross-section passing from small to large angles, the obtained spectra present essentially the same features and an acceptable signal to noise ratio. In particular the first inelastic peaks (0.844+1.015 MeV) are still distinguished from the elastic one.

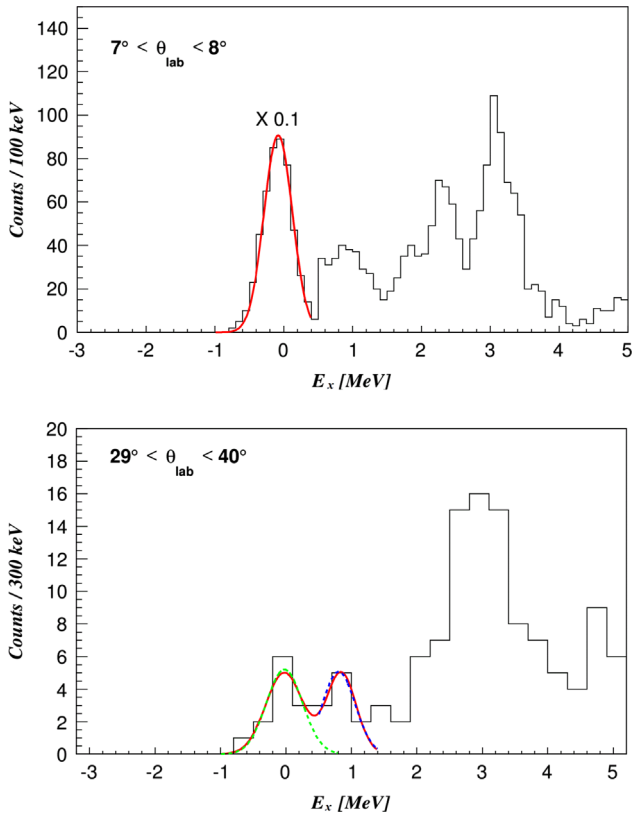

Fig. 4. ^{27}Al excitation energy spectra for two different scattering angles: (a) $7^\circ < \theta_{lab} < 8^\circ$, (b) $29^\circ < \theta_{lab} < 40^\circ$. The peak relative to the $^{27}Al_{g.s.}$ in the plot (a) has been scaled by a factor 0.1. The red solid line represents the overall result of the fit, the green- and blue-dashed lines are the individual Gaussian functions extracted from the fit.(For interpretation of the references to color in this figure legend, the reader is referred to the web version of this article.)

4. Cross-section angular distributions

For an accurate measurement of the rapidly oscillating angular distributions, characteristic of the elastic and inelastic processes studied here, several conditions need to be fulfilled. The systematic error in the absolute value of the cross-sections should be about 10% or less to discriminate among different theoretical predictions. Particular care should also be taken with the reduction of statistical errors and the uncertainties in the normalization. In addition, a proper description of the oscillating patterns, whose period is about 2° in the laboratory frame for the ^{16}O+^{27}Al elastic scattering at 280 MeV, requires that the experimental angular resolution should be maintained at least below 0.5°. The accuracy should be kept to that level for a useful comparison with the theoretical predictions.

The analysis of the kinematic lines shown in Fig. 3 does allow to check the accuracy in the reconstruction of the experimental laboratory angle θ_{lab}. As an example, the crossing point of the ^{27}Al (^{16}O, ^{16}O) $^{27}Al_{2.982}$ inelastic locus with the ^{16}O+^{16}O elastic one only depends on the beam energy. The discrepancy between the kinematic predictions and the experimental data is within 0.1°. This is in agreement to what was previously found for the

spectrometer at lower energies [12] and it is good enough to safely determine the position of the minima in the oscillating angular distributions.

The absolute cross-sections were extracted from the measured yield of the different levels in the energy spectra. The solid angle was carefully determined for the full spectrometer acceptance taking into account the overall transport efficiency as described in Ref. [20]. A measured dead-time fraction ranging from 13% to 39% (for the run at the highest beam current) was also accounted for. Fig. 5 shows the angular distributions of the absolute cross-section for the transition to the ^{27}Al ground and the excited states at 0.844 ($J_\pi=1/2^+$), 1.014 ($J_\pi=3/2^+$), 2.212 ($J_\pi=7/2^+$), 2.735 ($J_\pi=5/2^+$) and 3.00 MeV ($J_\pi=9/2^+$) for the different experimental runs. An angular bin of 0.2° was chosen for θ_{lab} for the data-set at $\theta_{opt}=10°$, 13° and 18°. This was raised to 0.5° at $\theta_{opt}=26°$ and to 1° at $\theta_{opt}=34°$ in order to achieve a good compromise between the statistical uncertainties in the number of counts for each bin and the angular resolution. The error bar in the absolute cross-section includes both a statistical contribution (between 1% at forward angles and 50% at the backward ones) and a component due to the uncertainty in the solid angle determination. The latter gives a not negligible contribution only at the borders of the accepted phase space, namely the first and last two bins in the angular distributions for each run, where it reaches values as high as 30%. An overall systematic error of about 10% is estimated, mainly due to the uncertainties on the target thickness. A more detailed analysis of the errors in the differential cross-section is reported in Ref. [20].

The excited states considered in Fig. 5 form a multiplet ($1/2^+$, $3/2^+$, $5/2^+$, $7/2^+$ and $9/2^+$) characterized by the dominant ^{28}Si ($J^\pi=2^+$; $E^*=1.7$ MeV) $\otimes$ $\pi(1d_{5/2})^{-1}$ configuration [21,22], where the collective 2^+ excited state of ^{28}Si couples with a $1d_{5/2}$ proton hole. A $3/2^+$ state at 2.984 MeV is in principle populated, but was not observed in previous inelastic scattering experiments and we omitted it from the discussion. The states of the multiplet are properly described within a weak coupling model, which predicts the same response as for the ^{28}Si(2^+) collective state. Since the L-transfer is the same within the multiplet ($L=2$ from ^{28}Si(0^+) to ^{28}Si(2^+)) the angular distributions have the same shape. This was observed in inelastic scattering of protons, deuterons and α particles (see [23] and references therein). We also find this behavior in the comparison of the angular distributions of the unresolved 0.844–1.014 MeV states, 2.212 MeV state and the unresolved 2.735–3.004 MeV states. The shape of the summed inelastic cross-sections of Fig. 5 resembles therefore to that of the individual contributions. The angular distribution for the elastic scattering oscillates in opposition of phase compared to the inelastic transitions, similar to what was found in Ref. [2]. This behavior is typical for heavy-ion elastic and inelastic scattering [24].

Thanks to the large angular acceptance of the spectrometer, significant overlaps between the two measurements at adjacent angles are available, thus allowing a supplementary check of the quality of the absolute measurement of the cross-section. The observed agreement in the overlap region is excellent both in the elastic and inelastic channels. All of this confirms the reliability of the instrument for this kind of study. It should be noticed that the measured differential cross-section for the elastic scattering ranges from 10^4 mb/sr at forward angles and decreases to almost 10 nb/sr at backward angles range, thus covering an interval of about eight orders of magnitude.

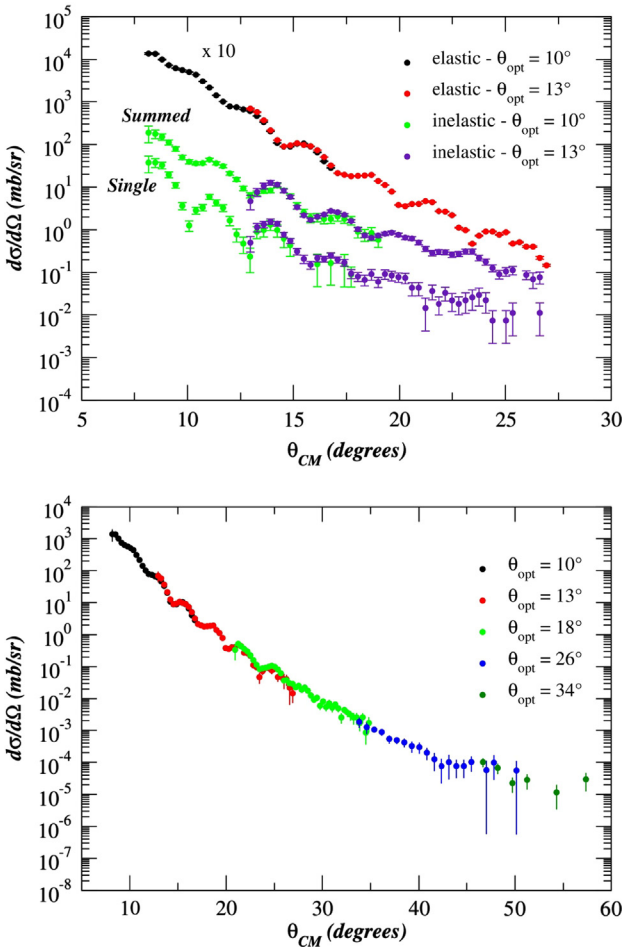

Fig. 5. Angular distributions of the differential cross-section in the center of mass reference frame. Upper panel: ^{16}O+^{27}Al elastic, sum of the inelastic transitions to the 0.844, 1.014, 2.212, 2.735 and 3.004 MeV states (summed) and inelastic transitions to 2.735 and 3.004 MeV states (single) at $\theta_{opt}=10°$ and $\theta_{opt}=13°$. Lower panel: ^{16}O+^{27}Al elastic in the whole explored angular range.

5. Conclusions

The ^{16}O+^{27}Al elastic and inelastic scattering was measured at 280 MeV incident energy using the MAGNEX spectrometer. A careful tuning of the SC accelerator and the transport line allowed the selection of a single turn, low emittance and considerable intensity beam on the target. Thanks to the large solid angle, a broad angular range was explored in the five different exposures. The application of the ray reconstruction technique allowed the reach of high mass, energy and angular resolution. As a consequence all the challenging requirements of the experiment were satisfied for the first time, allowing the unambiguous identification of the ^{16}O ejectiles, the separation of the ground from the first excited state of ^{27}Al at 844 keV and the accurate determination of absolute cross-sections and angular distributions even at backward angles.

We emphasize that the cross-section decreases by about eight orders of magnitude in the explored angular region, down to about 10 nb/sr, a condition much more stringent than at lower incident energy [2,18]. The accomplishment of such results is an encouraging issue opening many-fold perspectives in a novel class of high resolution studies of heavy-ion processes at intermediate energies [25,26]. The described technique is in fact general enough to be easily applied to many other systems in a broad energy range.

Acknowledgments

The authors wish to acknowledge the INFN-LNS acceleration division staff for the excellent job done in setting up the beam according to the stringent requirements of the experiment.

References

[1] D. Pereira, et al., Physics Letters B 670 (2009) 330.
[2] D. Pereira, et al., Physics Letters B 710 (2012) 426.
[3] J.R.B. Oliveira, et al., Journal of Physics G: Nuclear and Particle Physics 40 (2013) 105101.
[4] D. Pereira, et al., AIP Conference Proceedings 1491 (2012) 353.
[5] L. Bianchi, et al., Nuclear Instruments and Methods in Physics Research Section A 509 (1989).
[6] M. Fujiwara, et al., Nuclear Instruments and Methods in Physics Research Section A 422 (1999) 484.
[7] M. Cavallaro, et al., Physical Review C 88 (2013) 054601.
[8] D. Rifuggiato, et al., in : Proceedings of the XVII International Conference on Cyclotrons and their Applications, Tokyo, Japan, 2004, 118.
[9] F. Cappuzzello, et al., MAGNEX: an innovative large acceptance spectrometer for nuclear reaction studies in: Magnets: Types, Uses and Safety, Nova Publisher Inc., New York (2011) 1–63.
[10] A. Cunsolo, et al., Nuclear Instruments and Methods in Physics Research Section A 481 (2002) 48.
[11] A. Cunsolo, et al., Nuclear Instruments and Methods in Physics Research Section A 484 (2002) 56.
[12] F. Cappuzzello, et al., Nuclear Instruments and Methods in Physics Research Section A 638 (2011) 74.
[13] M. Cavallaro, et al., European Physical Journal A 48 (2012) 59.
[14] C. Boiano, et al., IEEE Transactions on Nuclear Science NS55 (2008) 3563.
[15] F. Cappuzzello, et al., Nuclear Instruments and Methods in Physics Research Section A 621 (2010) 419.
[16] D. Carbone, et al., European Physical Journal A 48 (2012) 60.
[17] A. Lazzaro, et al., Nuclear Instruments and Methods in Physics Research Section A 602 (2009) 494.
[18] M. Cavallaro, et al., Nuclear Instruments and Methods in Physics Research Section A 648 (2011) 46.
[19] J.F. Ziegler, et al., Nuclear Instruments and Methods in Physics Research Section B, Volume 268, Issue 11-12, p. 1818-1823..
[20] M. Cavallaro, et al., Nuclear Instruments and Methods in Physics Research Section A 637 (2011) 77.
[21] P.M. Endt, et al., Nuclear Physics A 521 (1990) 1.
[22] G.M. Crawley, G.T. Garvey, Physics Letters 19 (1965) 229.
[23] G.M. Crawley, G.T. Garvey, Physical Review 167 (1968) 1070.
[24] G.R. Satchler, W.G. Love, Physics Reports 55 (1979) 183.
[25] T. Uesaka, et al., Progess of Theoretical Physics 196 (2012) 150.
[26] H. Matsubara, et al., Few-Body Systems 54 (2013) 1433.